Guidance of a Human Driver by an Automated Vehicle: Nonlinear Control Design via Delayed Spectral Submanifold

Bence Szaksz, Nathan van de Wouw, *Fellow, IEEE*, Gábor Stépán, and Gábor Orosz, *Senior Member, IEEE*

***Abstract*— This letter investigates a specific human-machine interaction in which an automated vehicle (AV) provides guided control to a following human-driven vehicle (HV). We take into account both the state delay induced by human reaction time and the input delay introduced by the AV controller. The resulting dynamic model is a nonlinear delay differential equation (DDE) with two distinct constant time delays. Our objective is to design a controller for this infinite-dimensional system at the nonlinear level. First, a model reduction is performed using the delayed spectral submanifold approach. This allows us to project the dynamics onto a low-dimensional invariant manifold while capturing the essential nonlinear behavior. Based on this reduced-order model, we then design a nonlinear controller that achieves faster convergence compared to a purely linear controller. The benefits of the proposed approach for closed-loop performance are demonstrated through numerical simulations.**

***Index Terms*— Autonomous vehicles, model/controller reduction, nonlinear output feedback, delay systems.**

I. Introduction

AUTOMATED vehicles (AVs) with properly designed control have the potential to benefit not only their own performance but also that of the surrounding human-driven vehicles (HVs). Several field experiments demonstrated that a single AV can dissipate human-induced oscillations in mixed traffic situations [1], [2], [3]. Despite these successes, designing effective AV controllers for mixed traffic situations remains a challenging task due to the inherently nonlinear human driving behavior and the presence of relevant time delays.

Received 17 March 2026; revised 16 May 2026; accepted 25 May 2026. Date of publication 5 June 2026; date of current version 2 July 2026. The work of Bence Szaksz was supported in part by the Roszkoczy Foundation and in part the Eötvös Hungarian State Scholarship funded by the Ministry of Culture and Innovation of Hungary. This article has not been presented at a conference. Recommended by Senior Editor R. Vazquez. *(Corresponding author: Bence Szaksz.)*

Bence Szaksz is with the Department of Mechanical Engineering, University of Michigan, Ann Arbor, MI 48109 USA, and also with the Department of Applied Mechanics, Faculty of Mechanical Engineering, Budapest University of Technology and Economics, 1111 Budapest, Hungary (e-mail: szaksz@mm.bme.hu).

Nathan van de Wouw is with the Department of Mechanical Engineering, Eindhoven University of Technology, 5600 MB Eindhoven, The Netherlands (e-mail: N.v.d.Wouw@tue.nl).

Gábor Stépán is with the Department of Applied Mechanics and the HUN-REN–BME Dynamics of Machines Research Group, Budapest University of Technology and Economics, 1111 Budapest, Hungary (e-mail: stepan@mm.bme.hu).

Gábor Orosz is with the University of Michigan, Ann Arbor, MI 48109 USA (e-mail: orosz@umich.edu).

Digital Object Identifier 10.1109/LCSYS.2026.3700684

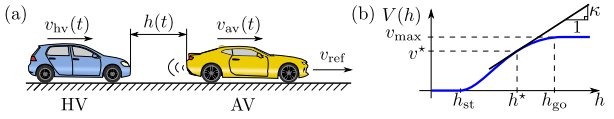

Fig. 1. Panel (a) presents the guided control scenario, while panel (b) depicts the nonlinear range policy of the human driver.

These systems are governed by nonlinear delay differential equations (DDEs) that have an infinite-dimensional state-space [4]. To facilitate control design, model order reduction can be carried out leading to reduced number of DDEs [5] or finite-dimensional approximations [6]. For DDEs, the conventional Lyapunov-Krasovskii functional-based control design remains technically challenging and often offers conservative results [7], while discretization-based approximations cannot capture the delayed nature in detail. Instead, here we determine a *finite-dimensional* reduced dynamics on a dominant invariant manifold that is calculated analytically without destructive discretization. This is facilitated by the delayed spectral submanifold (SSM) calculation [8], [9], which is based on the earlier results for ordinary differential equations [10].

In this letter, we present a delayed-SSM-based nonlinear control design for a human-machine interaction scenario in which an AV provides guidance to a following HV, see Fig. 1. This system has previously been investigated for a linear AV control strategy, however, under the restriction of identical delays for the AV and HV [11], [12]. Here, we generalize the delayed SSM calculation to the case of multiple distinct delays, which requires careful treatment of the history space and especially the adjoint eigenfunctions. This enables us to differentiate the state delay induced by human reaction time and the input delay in the AV's control. The coefficients in the reduced dynamics can be expressed in closed form as functions of the nonlinear control gains, enabling nonlinear control design by directly tuning the reduced dynamics. In contrast to the predictor feedback method [13], our goal is to improve the transient performance, when local stability is already ensured. In this way, the letter proposes a constructive and generalizable control design technique at the nonlinear level for systems with multiple delays.

The letter is organized as follows. Section II introduces the guided control model, while Sec. III discusses the SSM

calculation, including the mathematical background of sun-star calculus and the projection of the dynamics to a two-dimensional manifold. Section IV introduces the nonlinear controller tuning, which is followed by an illustrative case study in Sec. V. Finally, Sec. VI summarizes the results.

II. Problem Statement

Consider a human-machine interaction where an AV tracks a reference velocity v_{ref}, while it also provides guidance to a following HV. In particular, the AV aims to create an easy-to-follow motion for the HV. The corresponding car-following setup is illustrated in Fig. 1(a). The velocities of the AV and the HV are denoted by v_{av} and v_{hv}, respectively, while the distance between the two vehicles is h. While the corresponding linear control strategy was investigated via human-in-the-loop experiments in [14], here, we focus on nonlinear control design. More details on AV control in mixed traffic can be found in [15] and [16].

The corresponding governing equations take the form

$$\begin{aligned} \dot{h}(t) &= v_{\mathrm{av}}(t) - v_{\mathrm{hv}}(t)\,, \\ \dot{v}_{\mathrm{hv}}(t) &= f_{\mathrm{hv}}(h(t-\tau), v_{\mathrm{hv}}(t-\tau), v_{\mathrm{av}}(t-\tau))\,, \\ \dot{v}_{\mathrm{av}}(t) &= u(t-\sigma)\,, \end{aligned} \tag{1}$$

where $f_{\mathrm{hv}}(h, v_{\mathrm{hv}}, v_{\mathrm{av}})$ models the nonlinear dynamics of the human-driven vehicle, while $u(t-\sigma)$ is the controller of the AV to be designed. The state delay τ comes from human reaction time, while the input delay σ arises from the AV control loop. We adopt the car-following model from [16]:

$$f_{\mathrm{hv}}(h, v_{\mathrm{hv}}, v_{\mathrm{av}}) = \alpha(V(h) - v_{\mathrm{hv}}) + \beta(v_{\mathrm{av}} - v_{\mathrm{hv}})\,, \tag{2}$$

with gains α and β, and with the nonlinear range policy

$$V(h) = \begin{cases} 0, & \text{if } h \le h_{\mathrm{st}}\,, \\ v_{\max}\dfrac{(3h_{\mathrm{go}} - h_{\mathrm{st}} - 2h)(h-h_{\mathrm{st}})^2}{(h_{\mathrm{go}} - h_{\mathrm{st}})^3}, & \text{if } h_{\mathrm{st}} < h < h_{\mathrm{go}}\,, \\ v_{\max}, & \text{if } h \ge h_{\mathrm{go}}\,, \end{cases} \tag{3}$$

which is depicted in Fig. 1(b).

We search for a nonlinear control law in the form

$$u = f_{\mathrm{av}}(v_{\mathrm{hv}}, v_{\mathrm{av}}) = \sum_{k=1}^{3} \hat{\beta}_k (v_{\mathrm{ref}} - v_{\mathrm{av}})^k + \tilde{\beta}_k (v_{\mathrm{hv}} - v_{\mathrm{av}})^k, \tag{4}$$

that expresses the AV's intention to follow the reference speed v_{ref} (using gains $\hat{\beta}_k$, $k = 1, 2, 3$), while trying to match the speed of the following HV (using gains $\tilde{\beta}_k$, $k = 1, 2, 3$). A third-order law is used as it is the lowest order that facilitates the nonlinear control design discussed in Sec. IV.

Consider the steady-state solution when both vehicles travel with $v_{\mathrm{ref}} \in (0, v_{\max})$, that is, $v^\star_{\mathrm{hv}}(t) = v^\star_{\mathrm{av}}(t) \equiv v_{\mathrm{ref}}$, while the corresponding headway is $h^\star = V^{-1}(v^\star_{\mathrm{hv}})$. Let us consider perturbation coordinates with respect to the equilibrium by $\tilde{h} = h - h^\star$, $\tilde{v}_{\mathrm{hv}} = v_{\mathrm{hv}} - v^\star_{\mathrm{hv}}$, $\tilde{v}_{\mathrm{av}} = v_{\mathrm{av}} - v^\star_{\mathrm{av}}$, and introduce the state vector $\mathbf{x} = [\,\tilde{h}\ \tilde{v}_{\mathrm{hv}}\ \tilde{v}_{\mathrm{av}}\,]^\top$. In this way, the closed-loop dynamics is governed by the DDE

$$\begin{aligned} &\dot{\mathbf{x}}(t) \\ &= \mathbf{A}_0\mathbf{x}(t) + \mathbf{A}_\tau\mathbf{x}(t-\tau) + \mathbf{A}_\sigma\mathbf{x}(t-\sigma) + \mathbf{n}(\mathbf{x}(t-\tau), \mathbf{x}(t-\sigma)), \end{aligned} \tag{5}$$

with

$$\begin{aligned} \mathbf{A}_0 &= \begin{bmatrix} 0 & -1 & 1 \\ 0 & 0 & 0 \\ 0 & 0 & 0 \end{bmatrix}, \quad \mathbf{n}(\mathbf{x}(t-\tau), \mathbf{x}(t-\sigma)) = \begin{bmatrix} 0 \\ n_{\mathrm{hv}}(\mathbf{x}(t-\tau)) \\ n_{\mathrm{av}}(\mathbf{x}(t-\sigma)) \end{bmatrix}, \\ \mathbf{A}_\tau &= \begin{bmatrix} 0 & 0 & 0 \\ \alpha\kappa & -\alpha-\beta & \beta \\ 0 & 0 & 0 \end{bmatrix}, \quad \mathbf{A}_\sigma = \begin{bmatrix} 0 & 0 & 0 \\ 0 & 0 & 0 \\ 0 & \hat{\beta}_1 & -\hat{\beta}_1 - \tilde{\beta}_1 \end{bmatrix}, \end{aligned} \tag{6}$$

where $\kappa = V'(h^\star)$ is the slope of the range policy (see Fig. 1(b)), while the nonlinear functions take the form

$$\begin{aligned} n_{\mathrm{hv}}(\mathbf{x}(t-\tau)) &= \frac{1}{2}\alpha V''(h^\star)x_1^2(t-\tau) + \frac{1}{6}\alpha V'''(h^\star)x_1^3(t-\tau), \\ n_{\mathrm{av}}(\mathbf{x}(t-\sigma)) &= \tilde{\beta}_2(x_2(t-\sigma) - x_3(t-\sigma))^2 + \hat{\beta}_2 x_3^2(t-\sigma) \\ &\quad + \tilde{\beta}_3(x_2(t-\sigma) - x_3(t-\sigma))^3 + \hat{\beta}_3 x_3^3(t-\sigma). \end{aligned} \tag{7}$$

Here, n_{hv} is derived via a Taylor series expansion for $h_{\mathrm{st}} < h < h_{\mathrm{go}}$.

In this letter, we aim to investigate whether and how the nonlinear control law in (4) can improve the transient response of the closed-loop dynamics (5), compared to a linear control law, while ensuring local asymptotic stability of the desired steady state. This is a challenging task for the nonlinear, multi-delay system (5). Therefore, we pursue a nonlinear model order reduction in the next section.

III. Spectral Submanifold Calculation

The delayed SSM reduction has been investigated in [8] and [12] for a single delay. Here, we extend the framework to the case of multiple delays and propose a nonlinear controller design based on the obtained reduced dynamics.

The characteristic matrix, associated to the linear part of (5), takes the form

$$\mathbf{\Delta}(\lambda) = \lambda\mathbf{I} - \mathbf{A}_0 - \mathbf{A}_\tau \mathrm{e}^{-\lambda\tau} - \mathbf{A}_\sigma \mathrm{e}^{-\lambda\sigma}\,, \tag{8}$$

leading to the transcendental characteristic equation

$$\begin{aligned} &\lambda^3 + ((\alpha+\beta)\lambda^2 + \alpha\kappa\lambda)\mathrm{e}^{-\lambda\tau} + (\hat{\beta}_1 + \tilde{\beta}_1)\lambda^2\mathrm{e}^{-\lambda\sigma} \\ &+ ((\beta\hat{\beta}_1 + \alpha\hat{\beta}_1 + \alpha\tilde{\beta}_1)\lambda + \alpha\kappa\hat{\beta}_1)\mathrm{e}^{-\lambda(\tau+\sigma)} = 0\,. \end{aligned} \tag{9}$$

This equation has infinitely many solutions, finitely many of which are located to the right of an arbitrary vertical line in the complex plane. This facilitates the projection of the infinite-dimensional dynamics onto a finite-dimensional dominant spectral subspace. Since (9) is a transcendental equation, the eigenvalues have to be approximated numerically. We use the semi-discretization method [17] followed by Newton iteration.

In this section, we utilize the sun-star calculus to reformulate the DDE as an operator differential equation (OpDE), which allows us to determine the dominant eigenfunctions. Then, the SSM calculation yields the invariant manifold in the space spanned by these dominant eigenfunctions as well as the reduced dynamics that forms the basis for the nonlinear control design in Sec. IV. In the following, without loss of generality, we consider $\tau \ge \sigma$, that is, the human reaction time is larger than the delay of the AV.

A. Sun-Star Calculus

Consider the Banach space $\mathcal{B} = \mathcal{C}([-\tau, 0], \mathbb{C}^3)$ with the supremum norm $|\cdot|_{\mathcal{B}} := |\cdot|_\infty$ and let us introduce the state vector

$$\mathbf{x}_t(\vartheta) = \mathbf{x}(t+\vartheta)\,,\ \ \vartheta \in [-\tau, 0]. \tag{10}$$

Then, the DDE (5) can be formulated as the OpDE:

$$\dot{\mathbf{x}}_t(\vartheta) = \mathcal{A}^{\odot\star}\mathbf{x}_t(\vartheta) + \mathcal{N}(\mathbf{x}_t(\vartheta)), \tag{11}$$

with the linear operator $\mathcal{A}^{\odot\star} : \mathcal{B} \to \mathcal{B}$ and the nonlinear operator $\mathcal{N} : \mathcal{B} \to \mathcal{B}$, taking the following forms, respectively:

$$\begin{aligned}
\mathcal{A}^{\odot\star}\mathbf{\Phi} &= \begin{cases} \dfrac{\mathrm{d}\mathbf{\Phi}}{\mathrm{d}\vartheta}(\vartheta)\,, & \text{if } \vartheta \in [-\tau, 0)\,, \\ \mathbf{A}_0\mathbf{\Phi}(0) + \mathbf{A}_\tau\mathbf{\Phi}(-\tau) + \mathbf{A}_\sigma\mathbf{\Phi}(-\sigma)\,, & \text{if } \vartheta = 0\,, \end{cases} \\
\mathcal{N}(\mathbf{\Phi}) &= \begin{cases} \mathbf{0}\,, & \text{if } \vartheta \in [-\tau, 0)\,, \\ \mathbf{n}(\mathbf{\Phi}(-\tau), \mathbf{\Phi}(-\sigma))\,, & \text{if } \vartheta = 0\,. \end{cases}
\end{aligned} \tag{12}$$

Separate the nonlinearity into second- and third-order terms (see [8], [18]) by considering

$$\mathcal{N}(\mathbf{\Phi}) = \frac{1}{2!}\mathbf{B}(\mathbf{\Phi}, \mathbf{\Phi}) + \frac{1}{3!}\mathbf{C}(\mathbf{\Phi}, \mathbf{\Phi}, \mathbf{\Phi}) \tag{13}$$

with

$$\begin{aligned}
\mathbf{B}(\mathbf{\Phi}, \mathbf{\Lambda}) &= \begin{cases} \mathbf{0}\,, & \text{if } \vartheta \in [-\tau, 0), \\ \mathbf{b}(\mathbf{\Phi}, \mathbf{\Lambda}), & \text{if } \vartheta = 0\,, \end{cases} \\
\mathbf{C}(\mathbf{\Phi}, \mathbf{\Lambda}, \mathbf{\Gamma}) &= \begin{cases} \mathbf{0}\,, & \text{if } \vartheta \in [-\tau, 0), \\ \mathbf{c}(\mathbf{\Phi}, \mathbf{\Lambda}, \mathbf{\Gamma}), & \text{if } \vartheta = 0\,. \end{cases}
\end{aligned} \tag{14}$$

Here, $\mathbf{b}$ and $\mathbf{c}$ are multilinear vector-valued functions of $\mathbf{\Phi}, \mathbf{\Lambda}, \mathbf{\Gamma} \in \mathcal{B}$ taking the form

$$\begin{aligned}
\mathbf{b}(\mathbf{\Phi}, \mathbf{\Lambda}) &= \begin{bmatrix} 0 \\ \alpha V''(h^\star)\Phi_1(-\tau)\Lambda_1(-\tau) \\ b_3(\mathbf{\Phi}, \mathbf{\Lambda}) \end{bmatrix}, \\
\mathbf{c}(\mathbf{\Phi}, \mathbf{\Lambda}, \mathbf{\Gamma}) &= \begin{bmatrix} 0 \\ \alpha V'''(h^\star)\Phi_1(-\tau)\Lambda_1(-\tau)\Gamma_1(-\tau) \\ c_3(\mathbf{\Phi}, \mathbf{\Lambda}, \mathbf{\Gamma}) \end{bmatrix}.
\end{aligned} \tag{15}$$

with

$$\begin{aligned}
b_3(\mathbf{\Phi}, \mathbf{\Lambda}) &= 2\tilde{\beta}_2\Big(\Phi_2(-\sigma)\Lambda_2(-\sigma) - \Phi_2(-\sigma)\Lambda_3(-\sigma) \\
&\quad - \Lambda_2(-\sigma)\Phi_3(-\sigma) + 2\Phi_3(-\sigma)\Lambda_3(-\sigma)\Big) \\
&\quad + 2\hat{\beta}_2\Phi_3(-\sigma)\Lambda_3(-\sigma)\,, \\
c_3(\mathbf{\Phi}, \mathbf{\Lambda}, \mathbf{\Gamma}) &= 6\tilde{\beta}_3\Big(\Phi_2(-\sigma)\Lambda_2(-\sigma)\Gamma_2(-\sigma) \\
&\quad - \Phi_2(-\sigma)\Lambda_2(-\sigma)\Gamma_3(-\sigma) - \Phi_2(-\sigma)\Lambda_3(-\sigma)\Gamma_2(-\sigma) \\
&\quad - \Phi_3(-\sigma)\Lambda_2(-\sigma)\Gamma_2(-\sigma) + \Phi_3(-\sigma)\Lambda_3(-\sigma)\Gamma_2(-\sigma) \\
&\quad + \Phi_3(-\sigma)\Lambda_2(-\sigma)\Gamma_3(-\sigma) + \Phi_2(-\sigma)\Lambda_3(-\sigma)\Gamma_3(-\sigma)\Big) \\
&\quad - 6\hat{\beta}_3\Phi_3(-\sigma)\Lambda_3(-\sigma)\Gamma_3(-\sigma)\,.
\end{aligned} \tag{16}$$

We refer to equations (25)–(28) in [8] for their derivation.

The eigenfunction $\mathbf{Q} \in \mathcal{B}$ corresponding to a particular eigenvalue λ, being a solution of (9), satisfies

$$\mathcal{A}^{\odot\star}\mathbf{Q} = \lambda\mathbf{Q}\,, \tag{17}$$

where both λ and $\mathbf{Q}$ are associated to the linear part of the dynamics. This leads to a boundary value problem (BVP) (cf. (12)), whose solution becomes

$$\mathbf{Q}(\vartheta) = \mathbf{q}\mathrm{e}^{\lambda\vartheta}\,, \tag{18}$$

with $\mathbf{q} \in \mathbb{C}^3$ spanning the right null space of the characteristic matrix:

$$\mathbf{\Delta}(\lambda)\mathbf{q} = \mathbf{0}\,, \tag{19}$$

with $\Delta(\lambda)$ as in (8). Here, $\mathbf{q}$ is determined up to a free scalar multiplier; we select its first component as 1 leading to

$$\mathbf{q} = \begin{bmatrix} 1 & -\frac{\lambda^2 + \lambda(\hat{\beta}_1 + \tilde{\beta}_1)\mathrm{e}^{-\lambda\sigma}}{\lambda + \hat{\beta}_1\mathrm{e}^{-\lambda\sigma}} & -\frac{\lambda\tilde{\beta}_1\mathrm{e}^{-\lambda\sigma}}{\lambda + \hat{\beta}_1\mathrm{e}^{-\lambda\sigma}} \end{bmatrix}^\top. \tag{20}$$

Note that this expression does not explicitly include τ. However, the eigenvalue λ, being the solution of the characteristic equation (9), incorporates the τ-dependence.

Then, let us introduce the adjoint space $\mathcal{B}^\star = \mathcal{C}([0, \tau], \mathbb{C}^3)$ and the adjoint operator $\mathcal{A}^\odot : \mathcal{B}^\star \to \mathcal{B}^\star$ that takes the form

$$\mathcal{A}^\odot\Psi = \begin{cases} \dfrac{\mathrm{d}\mathbf{\Psi}}{\mathrm{d}\zeta}(0)\,, & \text{if } \zeta = 0\,, \\ \dfrac{\mathrm{d}\mathbf{\Psi}}{\mathrm{d}\zeta}(\zeta) + \mathbf{\Psi}(0)\mathbf{A}_0\,, & \text{if } \zeta \in (0, \sigma)\,, \\ \dfrac{\mathrm{d}\mathbf{\Psi}}{\mathrm{d}\zeta}(\zeta) + \mathbf{\Psi}(0)(\mathbf{A}_0 + \mathbf{A}_\sigma)\,, & \text{if } \zeta \in [\sigma, \tau)\,, \\ \mathbf{\Psi}(0)(\mathbf{A}_0 + \mathbf{A}_\tau + \mathbf{A}_\sigma)\,, & \text{if } \zeta = \tau\,, \end{cases} \tag{21}$$

which follows from the results in [19]. Here, $\mathbf{\Psi} \in \mathcal{B}^\star$ and $\mathbf{\Psi}(0)$ is a row vector. Moreover, the domain on which the adjoint operator $\mathcal{A}^\odot$ acts is restricted:

$$\mathcal{D}(\mathcal{A}^\odot) = \left\{\mathbf{\Psi} \in \mathcal{B}^\star : \frac{\mathrm{d}\mathbf{\Psi}}{\mathrm{d}\zeta}(\tau) = \mathbf{0}\right\}. \tag{22}$$

We define the pairing $\langle ., . \rangle$ as

$$\langle \mathbf{\Psi}, \mathbf{\Phi} \rangle = \mathbf{\Psi}(0)\mathbf{\Phi}(0) + \int_{-\tau}^{0} \frac{\mathrm{d}\mathbf{\Psi}}{\mathrm{d}\zeta}(-\theta)\mathbf{\Phi}(\theta)\mathrm{d}\theta \tag{23}$$

with respect to which the operators $\mathcal{A}^\odot$ and $\mathcal{A}^{\odot\star}$ satisfy the adjoint property:$\langle \mathcal{A}^\odot\mathbf{\Psi}, \mathbf{\Phi} \rangle = \langle \mathbf{\Psi}, \mathcal{A}^{\odot\star}\mathbf{\Phi} \rangle$.

The eigenfunction $\mathbf{P} \in \mathcal{B}^\star$ of $\mathcal{A}^\odot$ corresponding to the eigenvalue λ satisfies

$$\mathcal{A}^\odot\mathbf{P} = \lambda\mathbf{P}\,. \tag{24}$$

This, again, results in a BVP, the solution of which is Equation (25), as shown at the bottom of the next page. Here, $\mathbf{p} \in \mathbb{C}^3$ is a row vector that spans the left nullspace of the characteristic matrix $\mathbf{\Delta}(\lambda)$, that is,

$$\mathbf{p}\mathbf{\Delta}(\lambda) = \mathbf{0}\,. \tag{26}$$

Selecting the second coordinate of $\mathbf{p}$ as the free variable leads to the form

$$\mathbf{p} = \begin{bmatrix} \frac{\alpha\kappa\mathrm{e}^{-\lambda\tau}}{\lambda}p_2 & p_2 & \frac{(\alpha\kappa + \lambda\beta)\mathrm{e}^{-\lambda\tau}}{\lambda^2 + \lambda(\hat{\beta}_1 + \tilde{\beta}_1)\mathrm{e}^{-\lambda\sigma}}p_2 \end{bmatrix}. \tag{27}$$

To facilitate later the projection of the dynamics, the eigenfunctions $\mathbf{P}$ and $\mathbf{Q}$ are now normalized according to the pairing

$$\langle \mathbf{P}, \mathbf{Q} \rangle = 1\,. \tag{28}$$

which leads to

$$\mathbf{p}\mathbf{\Delta}'(\lambda)\mathbf{q} = 1\,, \tag{29}$$

where prime refers to the derivative with respect to λ. Equation (29) can be solved for p_2 resulting in a lengthy expression that is not presented here.

Finally, pairing the solution $\mathbf{x}_t$ with $\mathbf{P}$ projects the state onto the eigenfunction $\mathbf{Q}$, which defines the spectral coordinate

$$\eta(t) = \mathbf{p}\Bigg(\mathbf{x}(t) + \int_{-\tau}^{0} \mathbf{A}_\tau \mathrm{e}^{-\lambda(\theta+\tau)}\mathbf{x}(t+\theta)\mathrm{d}\theta + \int_{-\sigma}^{0} \mathbf{A}_\sigma \mathrm{e}^{-\lambda(\theta+\sigma)}\mathbf{x}(t+\theta)\mathrm{d}\theta\Bigg). \tag{30}$$

B. Projection to a Two-Dimensional Manifold

In this section, we consider that the dominant eigenvalues (eigenvalues with the largest real part) of system (5) form a complex conjugate pair λ_1 and $\lambda_2 = \overline{\lambda}_1$ such that $\mathrm{Re}\lambda_{1,2} < 0$, and perform the corresponding two-dimensional delayed SSM calculation. Note that the continuous extension of the results at $\mathrm{Re}\lambda_{1,2} = 0$ yields the standard center manifold reduction [4].

Let the vectors $\mathbf{q}$ and $\mathbf{p}$ span the right and left nullspaces of $\mathbf{\Delta}(\lambda_1)$, respectively, and let η denote the coordinate along the eigenfunction $\mathbf{Q}(\vartheta) = \mathbf{q}\mathrm{e}^{\lambda_1\vartheta}$. Then, the invariant manifold corresponding to the selected 2-dimensional subspace, called a spectral submanifold, can be approximated with the truncated multivariable power series

$$\mathbf{W}(\eta,\overline{\eta};\vartheta) = \sum_{1\le k+l\le 3} \mathbf{W}_{kl}(\vartheta)\eta^k\overline{\eta}^l + \eta^4\,. \tag{31}$$

with the coefficients $\mathbf{W}_{kl} \in \mathcal{B}$ for $k,l \in \mathbb{N}$, $k+l = 1,2,3$. The corresponding reduced dynamics assumes the form

$$\dot{\eta} = \lambda_1\eta + \sum_{2\le k+l\le 3} \gamma_{kl}\eta^k\overline{\eta}^l, \quad \dot{\overline{\eta}} = \overline{\lambda}_1\overline{\eta} + \sum_{2\le k+l\le 3} \overline{\gamma}_{kl}\overline{\eta}^k\eta^l, \tag{32}$$

where the coefficients γ_{kl} will be obtained later.

Substituting $\mathbf{x}_t(\vartheta) = \mathbf{W}(\eta(t),\overline{\eta}(t);\vartheta)$ into the OpDE (11), one obtains the invariance equation

$$\frac{\partial \mathbf{W}(\eta,\overline{\eta};\vartheta)}{\partial\eta}\dot{\eta} + \frac{\partial \mathbf{W}(\eta,\overline{\eta};\vartheta)}{\partial\overline{\eta}}\dot{\overline{\eta}} = \mathcal{A}^{\odot\star}\mathbf{W}(\eta,\overline{\eta};\vartheta) + \mathcal{N}(\mathbf{W}(\eta,\overline{\eta};\vartheta))\,, \tag{33}$$

which can be evaluated using (31) and (32). Our goal is to perform a polynomial balance to this expanded invariance equation and solve the resulting BVPs for the coefficients of the SSM and reduced dynamics. The first-order terms yield the eigenvalue-eigenfunction equations:

$$\mathcal{A}^{\odot\star}\mathbf{W}_{10} = \lambda_1\mathbf{W}_{10}\,, \quad \mathcal{A}^{\odot\star}\mathbf{W}_{01} = \overline{\lambda}_1\mathbf{W}_{01}\,, \tag{34}$$

which means that $\mathbf{W}_{10} = \mathbf{Q}$ and $\mathbf{W}_{01} = \overline{\mathbf{Q}}$, obviously. Then, the polynomial balance of the second-order terms leads to

$$\begin{aligned}
(2\lambda_1\mathcal{I} - \mathcal{A}^{\odot\star})\mathbf{W}_{20} &= \frac{1}{2}\mathbf{B}(\mathbf{W}_{10},\mathbf{W}_{10}) \\
&\quad - \gamma_{20}\mathbf{W}_{10} - \overline{\gamma}_{02}\mathbf{W}_{01}\,, \\
((\lambda_1+\overline{\lambda}_1)\mathcal{I} - \mathcal{A}^{\odot\star})\mathbf{W}_{11} &= \mathbf{B}(\mathbf{W}_{10},\mathbf{W}_{01}) \\
&\quad - \gamma_{11}\mathbf{W}_{10} - \overline{\gamma}_{11}\mathbf{W}_{01}\,, \\
(2\overline{\lambda}_1\mathcal{I} - \mathcal{A}^{\odot\star})\mathbf{W}_{02} &= \frac{1}{2}\mathbf{B}(\mathbf{W}_{01},\mathbf{W}_{01}) \\
&\quad - \gamma_{02}\mathbf{W}_{10} - \overline{\gamma}_{20}\mathbf{W}_{01}\,.
\end{aligned} \tag{35}$$

These equations do not have a unique solution yet; first, we have to restrict the reduced dynamics coefficients [8], [10]. Impose the condition that $\langle \mathbf{P}, \mathbf{W}_{kl}\rangle = 0$, for $k,l \in \mathbb{N}$, $k+l = 2$, and perform the pairing between $\mathbf{P}$ and the equations in (35). These yield

$$\gamma_{20} = \frac{1}{2}\mathbf{p}\,\mathbf{b}(\mathbf{W}_{10},\mathbf{W}_{10})\,,\ \gamma_{11} = \mathbf{p}\,\mathbf{b}(\mathbf{W}_{10},\mathbf{W}_{01})\,,\ \gamma_{02} = \frac{1}{2}\mathbf{p}\,\mathbf{b}(\mathbf{W}_{01},\mathbf{W}_{01})\,. \tag{36}$$

Then, under the nonresonance conditions (see [8], [9])

$$\mathrm{Ker}((k\lambda_1 + l\overline{\lambda}_1)\mathcal{I} - \mathcal{A}^{\odot\star}) \neq \{0\}, \quad k+l = 2\,, \tag{37}$$

the solution of the BVPs (35) leads to

$$\begin{aligned}
\mathbf{W}_{20}(\vartheta) &= \frac{1}{2}\mathbf{\Delta}^{-1}(2\lambda_1)\,\mathbf{b}(\mathbf{W}_{10},\mathbf{W}_{10})\mathrm{e}^{2\lambda_1\vartheta} \\
&\quad - \frac{\gamma_{20}}{\lambda_1}\mathbf{q}\mathrm{e}^{\lambda_1\vartheta} - \frac{\overline{\gamma}_{02}}{2\lambda_1 - \overline{\lambda}_1}\overline{\mathbf{q}}\mathrm{e}^{\overline{\lambda}_1\vartheta}, \\
\mathbf{W}_{11}(\vartheta) &= \mathbf{\Delta}^{-1}(\lambda_1+\overline{\lambda}_1)\,\mathbf{b}(\mathbf{W}_{10},\mathbf{W}_{01})\mathrm{e}^{(\lambda_1+\overline{\lambda}_1)\vartheta} \\
&\quad - \frac{\gamma_{11}}{\overline{\lambda}_1}\mathbf{q}\mathrm{e}^{\lambda_1\vartheta} - \frac{\overline{\gamma}_{11}}{\lambda_1}\overline{\mathbf{q}}\mathrm{e}^{\overline{\lambda}_1\vartheta},
\end{aligned} \tag{38}$$

while $\mathbf{W}_{02}(\vartheta) = \overline{\mathbf{W}}_{20}(\vartheta)$.

The polynomial balance for the third-order terms yields

$$\begin{aligned}
\gamma_{30} &= \mathbf{p}\left(\mathbf{b}(\mathbf{W}_{10},\mathbf{W}_{20}) + \frac{1}{6}\mathbf{c}(\mathbf{W}_{10},\mathbf{W}_{10},\mathbf{W}_{10})\right), \\
\gamma_{21} &= \mathbf{p}\left(\mathbf{b}(\mathbf{W}_{10},\mathbf{W}_{11}) + \mathbf{b}(\mathbf{W}_{01},\mathbf{W}_{20}) + \frac{1}{2}\mathbf{c}(\mathbf{W}_{10},\mathbf{W}_{10},\mathbf{W}_{01})\right), \\
\gamma_{12} &= \mathbf{p}\left(\mathbf{b}(\mathbf{W}_{10},\mathbf{W}_{02}) + \mathbf{b}(\mathbf{W}_{01},\mathbf{W}_{11}) + \frac{1}{2}\mathbf{c}(\mathbf{W}_{10},\mathbf{W}_{01},\mathbf{W}_{01})\right), \\
\gamma_{03} &= \mathbf{p}\left(\mathbf{b}(\mathbf{W}_{01},\mathbf{W}_{02}) + \frac{1}{6}\mathbf{c}(\mathbf{W}_{01},\mathbf{W}_{01},\mathbf{W}_{01})\right).
\end{aligned} \tag{39}$$

The corresponding coefficients of the spectral submanifold can also be obtained under the nonresonance conditions

$$\mathrm{Ker}((k\lambda_1 + l\overline{\lambda}_1)\mathcal{I} - \mathcal{A}^{\odot\star}) \neq \{0\}, \quad k+l = 3\,, \tag{40}$$

but the lengthy algebraic expressions are omitted here. As the final formulas (36), (38), (39) (and also the formula for the third-order SSM coefficients) are independent of the dimension of the system (5), the approach is scalable.

$$\mathbf{P}(\zeta) = \begin{cases} \mathbf{p}\mathrm{e}^{\lambda\zeta}\,, & \text{if } \zeta = 0\,, \\ \mathbf{p}\left(\mathbf{I} + (\mathbf{A}_\tau\mathrm{e}^{-\lambda\tau} + \mathbf{A}_\sigma\mathrm{e}^{-\lambda\sigma})\dfrac{\mathrm{e}^{\lambda\zeta}-1}{\lambda}\right), & \text{if } \zeta \in (0,\sigma)\,, \\ \mathbf{p}\left(\mathbf{I} + \mathbf{A}_\tau\mathrm{e}^{-\lambda\tau}\dfrac{\mathrm{e}^{\lambda\zeta}-1}{\lambda} + \mathbf{A}_\sigma\mathrm{e}^{-\lambda\sigma}\dfrac{\mathrm{e}^{\lambda\sigma}-1}{\lambda}\right), & \text{if } \zeta \in [\sigma,\tau)\,, \\ \mathbf{p}\left(\mathbf{I} + \mathbf{A}_\tau\mathrm{e}^{-\lambda\tau}\dfrac{\mathrm{e}^{\lambda\tau}-1}{\lambda} + \mathbf{A}_\sigma\mathrm{e}^{-\lambda\sigma}\dfrac{\mathrm{e}^{\lambda\sigma}-1}{\lambda}\right), & \text{if } \zeta = \tau\,. \end{cases} \tag{25}$$

Finally, we define the nonlinear part of the SSM as

$$\mathbf{w}(\eta,\overline{\eta};\vartheta) = \mathbf{W}(\eta,\overline{\eta};\vartheta) - \eta\mathbf{Q}(\vartheta) - \overline{\eta}\overline{\mathbf{Q}}(\vartheta), \tag{41}$$

which will be used later for visualization purposes.

The spectral and polynomial truncation introduces inaccuracies [20]. The validity domain of the dynamics approximation is challenging to determine, especially since the dimension of the reduced dynamics is different from that of the original dynamics. Nevertheless, as Sec. V presents, a two-dimensional SSM of third-order can provide a reduced-order model of acceptable accuracy. Note that if resonance occurs, then the dominant spectral subspace must be extended to include the resonant eigenvalues, in which case the SSM can be obtained with appropriate transformations [20]. In summary, the spectral submanifold (31) together with the corresponding reduced dynamics (32) represents the two-dimensional reduced-order model. These are utilized below to tune the nonlinear AV controller in (4), aiming for faster convergence than a simple linear controller.

IV. Nonlinear Control Design

According to the characteristic equation (9), the dominant eigenvalues λ_1, λ_2 can be designed by tuning the coefficients $\hat{\beta}_1, \tilde{\beta}_1$ of the linear terms in the controller (4). We assume that these control gains are already fixed and focus on the control design at the nonlinear level. The direct controller tuning on the original nonlinear DDE (5) is challenging due to the presence of multiple delays. Here, we utilize the reduced-order model of Section III to support simpler tuning of the nonlinear controller for faster transient performance.

The coefficients γ_{kl} of the nonlinear terms in the reduced dynamics (32) are functions of the gains $\hat{\beta}_2$, $\tilde{\beta}_2$, $\hat{\beta}_3$, and $\tilde{\beta}_3$ (cf. (15), (16), (36), (39)). This allows one to design γ_{kl} and, subsequently, to calculate the corresponding gains $\hat{\beta}_i$, $\tilde{\beta}_i$, $i \in 2,3$. To facilitate this, we introduce the following theorem.

Theorem 1: Consider the reduced dynamics in the form of (32). Assume that the linear part of (32) is exponentially stable, that is, $\mathrm{Re}\lambda_1 < 0$, and introduce the variables $\rho, \varphi \in \mathbb{R}$ such that $\eta(t) = \rho(t)\mathrm{e}^{\mathrm{i}\varphi(t)}$. Then, fixing $\gamma_{kl} = 0$ for $\{k,l|k+l = 2,3\}$, $k \neq l+1$ while designing $\mathrm{Re}\gamma_{21} < 0$ yields

$$\rho(t) = \rho(0)\mathrm{e}^{\mathrm{Re}(\lambda_1)t}\sqrt{\frac{\mathrm{Re}(\lambda_1)}{\mathrm{Re}(\lambda_1)+\mathrm{Re}(\gamma_{21})\rho^2(0)(1-\mathrm{e}^{2\mathrm{Re}(\lambda_1)t})}}, \tag{42}$$

where the expression under the square root is strictly smaller than 1 for $\forall t > 0$, which guarantees faster convergence compared to the linear case (i.e., when $\gamma_{21} = 0$); namely $|\rho(t)| < |\rho(0)|\mathrm{e}^{\mathrm{Re}(\lambda_1)t}$, $\forall t > 0$.

Proof: Substituting $\eta(t) = \rho(t)\mathrm{e}^{\mathrm{i}\varphi(t)}$ into (32) yields

$$\dot{\rho}\mathrm{e}^{\mathrm{i}\varphi} + \mathrm{i}\rho\dot{\varphi}\mathrm{e}^{\mathrm{i}\varphi} = \lambda_1\rho\mathrm{e}^{\mathrm{i}\varphi} + \sum_{2\le k+l\le 3}\gamma_{kl}\mathrm{e}^{(k-l)\mathrm{i}\varphi}\rho^{k+l}, \tag{43}$$

and its complex-conjugate pair. Then, multiplying (43) by $\mathrm{e}^{-\mathrm{i}\varphi}$ and separating the real and imaginary parts result in

$$\begin{aligned}\dot{\rho} &= \mathrm{Re}(\lambda_1)\rho + \sum_{2\le k+l\le 3}\mathrm{Re}\big(\gamma_{kl}\mathrm{e}^{(k-l-1)\mathrm{i}\varphi}\big)\rho^{k+l},\\ \rho\dot{\varphi} &= \mathrm{Im}(\lambda_1)\rho + \sum_{2\le k+l\le 3}\mathrm{Im}\big(\gamma_{kl}\mathrm{e}^{(k-l-1)\mathrm{i}\varphi}\big)\rho^{k+l},\end{aligned} \tag{44}$$

where all nonlinear terms have a phase-dependent multiplier $\mathrm{e}^{(k-l-1)\mathrm{i}\varphi}$ except for the term with $k = l+1$, for which this multiplier simplifies to 1. Considering only this nonlinear term $\gamma_{21}\eta^2\overline{\eta}$, the radius and phase are governed by

$$\begin{aligned}\dot{\rho} &= \rho\big(\mathrm{Re}(\lambda_1) + \mathrm{Re}(\gamma_{21})\rho^2\big),\\ \dot{\varphi} &= \mathrm{Im}(\lambda_1) + \mathrm{Im}(\gamma_{21})\rho^2, \qquad \text{for } \rho \neq 0.\end{aligned} \tag{45}$$

Solving the first equation (see [21], [22]), the time evolution of the radius $\rho(t)$ can be expressed in the closed form (42). This completes the proof.■

Therefore, ideally, one would cancel the coefficients of the nonlinear terms except that associated with γ_{21} and tune its real part to an appropriate negative value. However, there are six complex coefficients to cancel, and thus, such tuning procedure would require $6\cdot 2+1 = 13$ free nonlinear control gains, while we have only four (cf. (4)). Note that $\mathrm{Im}\gamma_{21}$ does not influence the convergence rate.

To tackle this problem, we minimize the effect of the phase-dependent terms by reducing their coefficients. In particular, we define the objective functions

$$\begin{aligned}J_2(\hat{\beta}_2,\tilde{\beta}_2) &= |\gamma_{20}(\hat{\beta}_2,\tilde{\beta}_2)|^2 + |\gamma_{11}(\hat{\beta}_2,\tilde{\beta}_2)|^2 + |\gamma_{02}(\hat{\beta}_2,\tilde{\beta}_2)|^2,\\ J_3(\hat{\beta}_2,\tilde{\beta}_2,\hat{\beta}_3,\tilde{\beta}_3) &= |\gamma_{30}(\hat{\beta}_2,\tilde{\beta}_2,\hat{\beta}_3,\tilde{\beta}_3)|^2\\ &\quad + |\gamma_{12}(\hat{\beta}_2,\tilde{\beta}_2,\hat{\beta}_3,\tilde{\beta}_3)|^2 + |\gamma_{03}(\hat{\beta}_2,\tilde{\beta}_2,\hat{\beta}_3,\tilde{\beta}_3)|^2,\end{aligned} \tag{46}$$

which can be minimized sequentially.

Equations (15), (16), and (36) yield that J_2 is a quadratic function in $\hat{\beta}_2$, $\tilde{\beta}_2$. Thus, the optimal gains are given by

$$\frac{\partial J_2(\hat{\beta}_2,\tilde{\beta}_2)}{\partial\hat{\beta}_2} = 0 \quad \text{and} \quad \frac{\partial J_2(\hat{\beta}_2,\tilde{\beta}_2)}{\partial\tilde{\beta}_2} = 0. \tag{47}$$

Fixing $\hat{\beta}_2$ and $\tilde{\beta}_2$ based on (47), the objective function J_3 is quadratic in $\hat{\beta}_3$ and $\tilde{\beta}_3$. J_3 should be minimized under the constraint that $\mathrm{Re}\gamma_{21}$ takes a negative value for faster convergence, yielding the constrained optimization problem

$$\begin{aligned}&\min_{\hat{\beta}_3,\tilde{\beta}_3\in\mathbb{R}} J_3(\hat{\beta}_2,\tilde{\beta}_2,\hat{\beta}_3,\tilde{\beta}_3)\\ &\text{s.t.} \quad \mathrm{Re}(\gamma_{21}(\hat{\beta}_2,\tilde{\beta}_2,\hat{\beta}_3,\tilde{\beta}_3)) = -\mu,\end{aligned} \tag{48}$$

where $\mu > 0$ is a tuning parameter. Indeed, this strategy can be generalized to more free parameters.

V. Illustrative Case Study

We fix the human driving parameters in (2), (3) as $\alpha = 0.3\,\mathrm{s}^{-1}$, $\beta = 0.4\,\mathrm{s}^{-1}$, $v_{\max} = 30\,\mathrm{m/s}$, $v_{\mathrm{ref}} = 26.55\,\mathrm{m/s}$, $h_{\mathrm{go}} = 55\,\mathrm{m}$, $h_{\mathrm{st}} = 5\,\mathrm{m}$, while considering the delays $\tau = 1\,\mathrm{s}$, and $\sigma = 0.5\,\mathrm{s}$. We also set the linear control gains as $\hat{\beta}_1 = 1\,\mathrm{s}^{-1}$, $\tilde{\beta}_1 = -0.4\,\mathrm{s}^{-1}$ in the AV controller (4). Then, the dominant eigenvalues form the complex conjugate pair $\lambda_{1,2} = -0.094 \pm 0.833\,\mathrm{i}$, which is well separated from the third rightmost eigenvalue $\lambda_3 = -0.443$ yielding that the nonresonance conditions (37) and (40) are satisfied. First, we show the dynamics with linear AV control ($\hat{\beta}_2 = \tilde{\beta}_2 = \hat{\beta}_3 = \tilde{\beta}_3 = 0$) when only the human driving behavior introduces nonlinearity into the system. Second, we compare these results to the case when the controller of the AV is also nonlinear and is tuned according to Sec. IV.

For the linear AV controller, Fig. 2(a) shows the nonlinear part of the SSM (41) above the space spanned by the real and imaginary parts of the dominant eigenfunction. The solid purple curve depicts a particular trajectory, while the dashed pink curve is an approximate solution obtained via projecting the initial function to the SSM (cf. (30)), and then performing a time integration based on the reduced dynamics (32). The

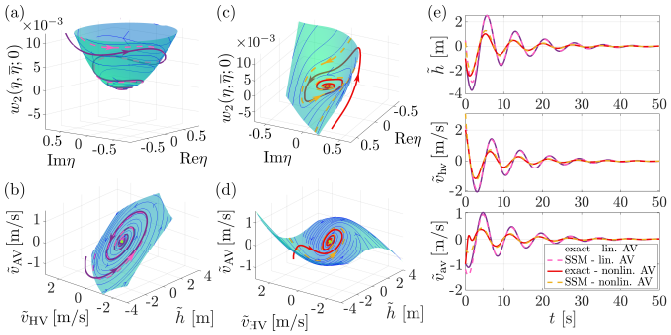

Fig. 2. Panels (a) and (c) show the second coordinate of the nonlinear part of the SSM above the space spanned by the real and imaginary parts of the dominant eigenfunction for the linear and for the nonlinear AV control strategy, respectively, while panels (b) and (d) present the same SSMs in the space of the physical coordinates. In panels (a) and (b) the solid purple and the dashed pink curves refer to the exact solution and its reduced-dynamics-based approximation for the linear control strategy, while in panels (c) and (d) the solid red and the dashed orange curves are the exact solution and its reduced-dynamics-based approximation for the nonlinear case. Panel (e) depicts the same trajectories as functions of time. All the trajectories are obtained for the initial condition $\tilde{v}_{hv}(t) \equiv 2\,\text{m/s}$, $\tilde{v}_{av}(t) \equiv -1\,\text{m/s}$, $\tilde{h}(0) = -1\,\text{m}$, and $\tilde{h}(t) = \tilde{h}(0) + (\tilde{v}_{av}(0) - \tilde{v}_{hv}(0))t$ for $t \in [-\tau, 0]$.

purple trajectory converges to the SSM and tends to the equilibrium along the predicted reduced-dynamics-based solution. Figure 2(b) presents the same objects in the space of the original physical coordinates, depicting the same convergence properties. The results show the effectiveness of the SSM-based model reduction.

The linear controller yields stable dynamics, but with slowly decaying transients. Let us now show how the appropriate selection of the nonlinear gains can improve the dynamical performance. Fixing $\mu = 0.1\,\text{s}^{-1}$, and solving the optimization problems (47), (48) results in $\hat{\beta}_2 = -0.007\,\text{m}^{-1}$, $\tilde{\beta}_2 = 0.004\,\text{m}^{-1}$, $\hat{\beta}_3 = -0.061\,\text{s/m}^2$, $\tilde{\beta}_3 = 0.070\,\text{s/m}^2$.

Figure 2(c) and (d) present the SSM of the resulting closed-loop system above the space of the real and imaginary parts of the dominant eigenvector and in the space of the physical coordinates. As can be seen, the SSM is more twisted in Fig. 2(d) than in Fig. 2(b), while they have a common tangential plane at the origin, because the linearized system is not modified. Solid red and dashed orange curves represent the time response of the system and the corresponding reduced-dynamics-based trajectory for the same initial condition as before. Again, the reduced dynamics provides a good prediction for the behavior of the real system. Figure 2(e) presents the evolution of the trajectories in time using the same color code. Clearly, the nonlinear AV control strategy results in a faster convergence than the simple linear strategy, showing the effectiveness of the above nonlinear control design procedure.

VI. Conclusion

In this letter, we introduced a nonlinear control design for systems with multiple delays utilizing the concept of spectral submanifolds (SSMs). Closed form algebraic expressions were given both for the spectral submanifold and for the corresponding reduced dynamics, which enabled the subsequent control design. A numerical case study demonstrated the effectiveness of the SSM-based time response prediction. Furthermore, the results showed that the proposed nonlinear control design can significantly improve the dynamic performance, resulting in faster convergence in our example.

The results provide a constructive method for the nonlinear control synthesis of complex systems with multiple time delays. Our future goal is to include additional nonlinear terms into the controller, which yields more flexibility in the tuning procedure, as well as to derive a general framework for multi-delay control systems. Besides, a detailed sensitivity study and extending the results to systems with distributed delay will also be considered.

References

[1] J. I. Ge, S. S. Avedisov, C. R. He, W. B. Qin, M. Sadeghpour, and G. Orosz, "Experimental validation of connected automated vehicle design among human-driven vehicles," *Transp. Res. C, Emerg. Technol.*, vol. 91, pp. 335–352, Jun. 2018.

[2] R. E. Stern et al., "Dissipation of stop-and-go waves via control of autonomous vehicles: Field experiments," *Transp. Res. C, Emerg. Technol.*, vol. 89, pp. 205–221, Apr. 2018.

[3] B. Szaksz, T. G. Molnar, S. S. Avedisov, G. Stepan, and G. Orosz, "Connected vehicle experiments on virtual rings: Unveiling bistable behavior," in *Proc. IEEE Intell. Vehicles Symp. (IV)*, Jun. 2025, pp. 1014–1019.

[4] G. Stépán, *Retarded Dynamical Systems*. White Plains, NY, USA: Longman, 1989.

[5] N. van de Wouw, W. Michiels, and B. Besselink, "Model reduction for delay differential equations with guaranteed stability and error bound," *Automatica*, vol. 55, pp. 132–139, May 2015.

[6] P. M. Mäkilä and J. R. Partington, "Shift operator induced approximations of delay systems," *SIAM J. Control Optim.*, vol. 37, no. 6, pp. 1897–1912, Jan. 1999.

[7] S. Li, R. Dong, and C. Wu, "Stabilization guarantees of human-compatible control via Lyapunov analysis," in *Proc. Eur. Control Conf. (ECC)*, Jun. 2023, pp. 1–8.

[8] B. Szaksz, G. Orosz, and G. Stepan, "Spectral submanifolds in time delay systems," *Nonlinear Dyn.*, vol. 113, no. 12, pp. 14265–14286, Jun. 2025.

[9] G. Buza and G. Haller, "Existence of spectral submanifolds in time delay systems," 2025, *arXiv:2512.22062*.

[10] G. Haller and S. Ponsioen, "Nonlinear normal modes and spectral submanifolds: Existence, uniqueness and use in model reduction," *Nonlinear Dyn.*, vol. 86, no. 3, pp. 1493–1534, Nov. 2016.

[11] B. Szaksz, G. Orosz, and G. Stépán, "Guided control of a human driver via an automated vehicle," *IFAC-PapersOnLine*, vol. 56, no. 2, pp. 899–904, 2023.

[12] B. Szaksz, G. Orosz, and G. Stepan, "Reduction to spectral submanifolds in guided car-following with time delay," *IFAC-PapersOnLine*, vol. 58, no. 27, pp. 67–72, 2024.

[13] N. Bekiaris-Liberis, C. Roncoli, and M. Papageorgiou, "Predictor-based adaptive cruise control design," *IEEE Trans. Intell. Transp. Syst.*, vol. 19, no. 10, pp. 3181–3195, Oct. 2018.

[14] B. Szaksz, G. Orosz, and G. Stepan, "Guided control of human drivers: Control design and experiments," *IEEE Trans. Control Syst. Technol.*, vol. 33, no. 6, pp. 2455–2462, Nov. 2025.

[15] T. G. Molnar and G. Orosz, "Destroying phantom jams with connectivity and automation: Nonlinear dynamics and control of mixed traffic," *Transp. Sci.*, vol. 58, no. 6, pp. 1319–1334, Nov. 2024.

[16] G. Orosz and T. G. Molnár, *Dynamics and Control of Connected Vehicles*. Cham, Switzerland: Springer, 2025.

[17] T. Insperger and G. Stepan, *Semi-Discretization for Time-Delay Systems: Stability and Engineering Applications*, vol. 178. New York, NY, USA: Springer, 2011.

[18] Y. A. Kuznetsov, *Elements of Applied Bifurcation Theory*. Cham, Switzerland: Springer, 1998.

[19] B. I. Wage, "Normal form computations for delay differential equations in DDE-BIFTOOL," Master's thesis, Fac. Sci., Universiteit Utrecht, Utrecht, The Netherlands, 2014.

[20] M. Li, S. Jain, and G. Haller, "Model reduction for constrained mechanical systems via spectral submanifolds," *Nonlinear Dyn.*, vol. 111, no. 10, pp. 8881–8911, May 2023.

[21] G. Teschl, *Ordinary Differential Equations and Dynamical Systems*. Providence, RI, USA: American Mathematical Soc., 2012.

[22] G. Orosz and A. D. Ames, "Safety functionals for time delay systems," in *Proc. Amer. Control Conf. (ACC)*, Jul. 2019, pp. 4374–4379.